WIND-TUNNEL INVESTIGATION OF A FULL-SCALE CANARD-CONFIGURED GENERAL AVIATION AIRCRAFT

ICAS-82-6.8.2

Long P. Yip, and Paul F. Coy
NASA Langley Research Center
Hampton, Virginia 23665

Abstract

As part of a broad research program to provide a data base on advanced airplane configurations, a wind-tunnel investigation was conducted in the Langley 30-by 60-Foot Wind Tunnel to determine the aerodynamic characteristics of an advanced canard-configured general aviation airplane. The investigation included measurements of forces and moments of the complete configuration, isolated canard loads, and pressure distributions on the wing, winglet, and canard. Flow visualization was obtained by using surface tufts to determine regions of flow separation and by using a chemical sublimation technique to determine boundary-layer transition locations. Additionally, other tests were conducted to determine simulated rain effects on boundary layer transition. Investigation of configuration effects included variations of canard locations, canard airfoil section, winglet size, and use of a leading-edge droop on the outboard section of the wing.

Symbols

b	wing span, ft
c	local chord, ft
$\bar{c}$	reference mean aerodynamic chord, 2.58 ft.
C_D	drag coefficient, drag/qS
C_L	lift coefficient, lift/qS
C_{L_α}	lift curve slope, per deg
C_ℓ	rolling-moment coefficient, rolling moment/qSb
C_{ℓ_β}	rolling moment due to sideslip, per deg
$C_{\ell_{\delta_a}}$	rolling-moment coefficient due to aileron deflection, per deg
C_m	pitching-moment coefficient, pitching-moment qSc
c_n	section normal-force coefficient, $\Sigma C_p \Delta(x/c)$
$C_{n_{\delta_a}}$	yawing-moment coefficient due to aileron deflection, per deg
$C_{n_{\delta_r}}$	yawing-moment coefficient due to rudder deflection, per deg
C_{n_β}	yawing moment due to sideslip
C_p	pressure coefficient, $p - p_\infty)/q$
i_c	incidence of canard, positive leading-edge up, deg
p	local static pressure, lb/ft^2
p_∞	freestream static pressure, lb/ft^2
q	freestream dynamic pressure, lb/ft^2
S	reference wing area, $53.6 ft^2$
V	freestream velocity, ft/sec
x,y,z	distances along body axes, ft
$(x/c)_T$	boundary-layer transition location
α	angle of attack, deg
β	angle of sideslip, deg
δ_a	aileron deflection, positive when right aileron is down, deg
δ_e	elevator deflection, positive when trailing edge is down, deg
δ_r	rudder deflection, positive when trailing edge is left, deg

Subscripts:

c	canard
l	lower surface
u	upper surface
w	winglet

Introduction

As part of the aeronautics research program at the NASA Langley Research Center, wind-tunnel tests were conducted in the Langley 30-by 60-Foot Wind Tunnel to determine the aerodynamic characteristics of a full-scale model of an advanced general aviation aircraft. The configuration was chosen for a baseline study because it incorporated many advanced design features, including: composite construction for light weight and smooth contours for maximum aerodynamic efficiency; winglets which provide directional stability and drag reduction; and a canard which was designed to limit the aircraft's ability to trim above the wing stall angle of attack (see reference 1). As As pointed out in reference 2, several factors such as canard size, aspect ratio, incidence setting, airfoil, propeller effects, and c.g. travel are important in designing a configuration that is not only stall proof but also statically stable and controllable. Tests were therefore conducted to provide a broad aerodynamic data base on canard configurations for use in the design of advanced aircraft. In addition to studies of the basic configuration, tests were conducted to determine the effects of canard height, canard incidence, canard airfoil section, winglets, leading-edge droop on the wing, and fixing boundary-layer transition on the canard. Flow-visualization studies were made with the use of tufts to determine regions of flow separation and a chemical sublimation technique was used to determine boundary-layer transition locations. Test conditions included an angle-of-attack range from -6° to 40° and an angle-of-sideslip range from -15° to +15° with freestream velocities that correspond to chord Reynolds numbers of up to 2.25 million.

Model Description and Test Conditions

The model used in the study was a full-scale model of a design intended for the homebuilt airplane market (reference 1). A full-scale model was constructed from foam section cutouts that were covered with fiberglass and epoxy, and a coat of body putty was used on the wing and canard to maintain airfoil section contours. Geometric characteristics of the model are given in Table I and shown in figure 1. Approximately 300 pressure ports were installed in the wing, canard, and winglet. Details of the pressure port locations are given in Table II. Photographs showing the model installed in the Langley 30-by 60-Foot Wind tunnel are presented in figures 2 and 3.

The basic configuration tested had the wing leading-edge droop installed, the nose gear retracted, main gear landing wheels exposed, and

the propeller removed. A low-drag, high lift airfoil section (referencd 3), incorporating a full-span slotted flap for pitch control was used on the canard. Elevator travel ranged from δ_e = -20° to +24°, and canard incidence was varied from i_c = -4° to +4°. A low canard position was also tested due to interest in improving pilot visibility. Tests were conducted with the leading-edge droop removed since earlier studies (references 4 and 5) indicated that the droop was effective in delaying tip stall. Larger winglets were also tested to provide an increase in the directional stability of the basic configuration. The larger winglets increased the original winglet area by 50-percent (see figure 1(b)).

Overall aerodynamic forces and moments acting on the model were measured on the external scale balance system of the Langley 30-by 60-Foot Wind Tunnel (see reference 6). In addition, the model was instrumented with internal strain-gage balances to measure isolated loads on the canard and propeller. In addition, pressure distributions were obtained using transducers. Small cotton tufts were used in conjunction with flourescent photography to provide flow visualization of the model. A chemical sublimation technique (see reference 7) was used to provide information on the extent of laminar flow on the canard, wing, and winglet. The engine inlet and exit area were sealed and faired for a no-flow-through condition for all testing except when the propeller was installed. The majority of the tests was conducted with the propeller removed.

The model was tested inverted to evaluate the flow angularity and strut tare corrections. An extensive wind-tunnel calibration was made prior to model installation to determine the horizontal buoyancy correction, and flow-field surveys ahead of the model were made in the manner of reference 8 to determine the flow blockage correction. These corrections have been applied to the data. Application of jet-boundary corrections was made in accordance with the method of reference 9.

Results and Discussion

Basic Aerodynamic Characteristics

Effect of Reynolds number.- Most of the tests were conducted at a freestream dynamic pressure of 10.5 lb/ft^2 which corresponds to a tunnel velocity of about 68 mph and a Reynolds number of about 1.6 x 10^6 based on $\bar{c}$ which is approximately the full-scale Reynolds number for landing approach speeds. However, in order to evaluate the sensitivity of the configuration to Reynolds number effects, tests were conducted at tunnel velocities corresponding to Reynolds numbers of 0.6 x 10^6 and 2.25 x 10^6 based on $\bar{c}$ on the leading-edge droop-off configuration. Results of the tests shown in figure 4, indicate that at low Reynolds number the canard lift was significantly reduced, resulting in a large nose-down pitching-moment increment. The loss of canard lift was probably due to the early laminar separation of the boundary layer on the canard. The Reynolds number data of 0.6 x 10^6 was unrealisticalcally low; however, the data are presented to illustrate the sensitivity of the specific canard airfoil to subcritical Reynolds number conditions, and the impact of laminar separation on configuration aerodynamics. At the higher Reynolds number conditions, the data of figure 5 are indicative of the surface-flow conditions at angles of attack up to complete wing stall. The canard was tufted in earlier tests; however, as will be discussed later, the tufts adversely affected the canard airfoil performance due to the laminar flow characteristics of the canard airfoil.

The tuft patterns of figure 5 show a classical development of spanwise flow near the trailing-edge for a swept wing. The development of spanwise flow which increases with angle of attack is a well-known phenomenon which usually results in flow separation at the wing tip. However, the outboard leading-edge droop of the present configuration acted as an aerodynamic boundary to prevent the spread of spanwise flow and delayed tip stall to a higher angle of attack. A comparison of the tuft patterns with and without leading-edge droop at α = 19.5° is shown in figure 6 to illustrate this effect. The effect of canard downwash on the wing is illustrated by the tuft photographs of figure 7. The tuft patterns of figure 7 indicate that the canard downwash helped to keep the flow attached on the inboard wing segment to a higher angle of attack. As will be discussed later, this downwash effect reduces the loading on the inboard section of the wing and delays wing stall to a higher angle of attack. An interesting effect on the wing was noted by the flow patterns on the middle row of tufts near mid-span of the wing at α = -0.5° (see figure 5(c)). This effect was caused by the impingement of the canard tip vortex on the wing, and the effect diminished at the higher angles of attack because the canard vortex was displaced to a higher location relative to the wing with increasing angle of attack. As shown in figure 8, with the canard in the low position the canard interference on the wing occurred at a higher angle of attack (α = 5.5°).

Pressure Distributions.- Presented in figure 9 are chordwise pressure distributions measured near the mid-span location of the wing, winglet, and canard. The data of figure 9 indicate that at α = 1.5°, favorable pressure gradients, which are conducive to boundary-layer stability and laminar flow, were obtained on the upper surface of the wing to 55-percent chord, on the winglet to 50-percent chord, and on the canard to 50-percent chord. The extent of favorable pressure gradient correlated well with the results of the boundary-layer transition study presented in later discussion.

Chordwise pressure distributions on the wing which were integrated to obtain the wing span load distribution are presented in figure 10 for angles of attack of α = 1.5° and α = 9.5°. A comparison of the span loading with and without the canard indicate that at both angles of attack the loading of the inboard wing was reduced due to the canard downwash while the loading of the wing outboard of the canard span was increased due to upwash associated with the canard tip vortex. These results are probably typical of canard configurations, illustrating the need for awareness of such aerodynamic interactions to obtain maximum wing efficiency and avoid wing tip stall induced by canard-induced upwash.

Effect of Configuration Features

Effect of Leading-Edge Droop.- As shown in the tuft photographs of figure 5, a wing leading-edge droop similar to that discussed in reference 4 delayed the tip stall of the wing to a higher angle of attack. A comparison of the basic configuration with and without leading-edge droop, shown in figure 11, indicates that the leading-edge droop significantly increased longitudinal static stability above $\alpha = 6°$. The increase in stability resulted from the increased attached flow near the wing tip due to the leading-edge droop. The effect of leading-edge droop on elevator deflection required for trimmed lift is shown in figure 12 for various c.g. locations. The data indicate that the leading-edge droop provided a larger stall margin, due in part to the increased $C_{L_{MAX}}$ with leading-edge droop on and in part to the increased stability which required more trim capability from the canard. The effect of leading-edge droop on trimmed drag characteristics, shown in figure 13, indicates a drag penalty of $\Delta C_D = 0.0040$ or about 4 knots at cruise speed of 150 knots. At climb lift coefficients, there was no drag penalty due to the leading-edge droop.

Effect of canard.- The aerodynamic effects of the canard are shown in figure 14 which presents lift, drag, and pitching-moment data for the canard-on and canard-off configurations. The canard forces and moments measured with the canard balance were subtracted from the canard-on configuration for analysis of wing aerodynamics. Comparison of lift data obtained for the canard-off configuration with data obtained by subtracting the canard lift (dashed line) shown in figure 14(a), indicate that the downwash of the canard caused the wing to produce less lift than the wing-alone configuration. This downwash effect also delayed wing stall to a higher angle of attack. A similar analysis of the drag polar, shown in figure 14(b), indicates that the canard had a beneficial effect on the wing at a cruise-lift coefficient of $C_L = .25$; however, the canard significantly increased drag of the wing above $C_L = 0.3$. The longitudinal stability of the complete configuration was characterized by three distinct changes in pitch stability with angle of attack, as shown in figure 14(c). The first change occurred at about $\alpha = 4°$ where there is a reduction in stability due to the decrease in C_{L_α} of the wing. This decrease in the lift curve slope was caused by the previously-discussed spanwise flow due to wing sweep which degraded the lift performance of the wing section. Since the reduction in longitudinal stability was related to the aerodynamics of the wing, the change in pitch stability can also be seen in the wing alone case. The second change in pitch stability occurred at about $\alpha = 14°$ where a significant increase in pitch stability occured due to canard stall. This nose down pitching-moment change provides the configuration with an aerodynamic limiting effect on pitch trim and stall departure. The third change in pitch stability occurred at about $\alpha = 22°$ where wing stall caused a destabilizing break in the pitching-moment curve.

Elevator effectiveness.- The effect of deflecting the canard elevator are presented in figure 15 for the basic configuration at the design aft-c.g. location (FS 102). As expected, The data of figure 15 indicate that positive elevator deflections are required to trim a canard configuration, resulting in increased overall lift. However, analysis of the canard balance lift and the total lift indicates that the canard lift was not directly additive due to the increased downwash of the canard on the wing. Maximum trim angle of attack is influenced by canard stall, which limits the capability of the canard to trim out pitching moments at higher angles of attack. For the basic canard incidence of 0°, canard stall occurred at about $\alpha = 14°$, and the maximum trim angle of attack for the aft-c.g. location was about $\alpha = 17°$ with the elevator at $_e = 15°$. Increasing elevator deflection angle to 20° or 24° actually decreased the maximum trim angle of attack due to decreased elevator effectiveness in stalled flow. Thus, maximum trim angle of attack was significantly less than the wing stall angle of attack, which resulted in increased inherent stall resistance.

Effect of canard incidence.- In order to obtain an inherently stall-proof canard configuration, it is important that the canard incidence is set so that the canard will stall at a lower angle of attack than the main wing. Test results of the configuration with canard incidences of -4° and +4° are shown in figure 16. As expected, the canard incidence affected the pitching-moment at zero lift and the angle of attack for canard stall. The configuration with canard incidence of +4° did not have the nonlinear pitching-moment characteristics at low angle of attack noted for the configuration with the canard at -4°. This effect was probably due to the combination of increase in downwash on the wing and the early stall angle of the canard for $i_c = +4°$. Trimmed elevator positions plotted against lift coefficient, shown in figure 17, indicate, that elevator effectiveness was reduced for the configuration with canard incidence of +4°. This reduction in elevator effectiveness is probably due to the elevator operating in a stalled-flow region above $\alpha = 8°$.

Effect of canard airfoil.- The stall characteristics of the canard might be expected to have a large effect on the longitudinal stability of a canard configuration. Therefore, a canard with a NACA 0012 airfoil section was also tested for comparison with results obtained with the basic airfoil section, GU25-8(11)5. In contrast to the NACA section, the basic GU airfoil section was relatively thick and highly cambered. Test results shown in figure 18, indicate that, as expected, the uncambered NACA 0012 section did not produce as much lift at $\alpha = 0°$. Also, the canard with the NACA 0012 stalled more abruptly and at a lower angle of attack; and that the canard gradually gained lift in the post-stall angle-of-attack range. This gradual increase in lift contributed to a post-stall pitch-up tendency for the modified configuration. In a condition corresponding to a more aft-c.g. location (.20c aft), as shown by the data of figure 19, this pitch-up characteristic could possibly lead to a deep-stall trim condition.

Effect of canard location.- In order to provide better pilot visibility, the canard was placed in a lower position (see figure 20). As indicated by the tuft photographs of figure 8, an interference effect of the tip vortex of the canard on

the wing was noted at $\alpha = 5.5°$ for the low canard configuration. Results from tests of this configuration, shown in figure 21, indicate only a small destabilizing effect in pitch in the angle-of-attack range from $\alpha = 6°$ to 14°. This destabilizing effect was probably caused by the interaction of the tip vortex flow of the canard with the main wing. Trimmed drag characteristics, shown in figure 22, indicate that at cruise-lift condition ($C_L = .25$), drag of the low-canard configuration was about the same as that of the high-canard configuration. At higher-lift coefficients, there was a slight increase in drag for the low-canard configuration. Although the data indicate only a slight effect of the canard tip vortex on the static aerodynamic characteristics of the configuration, further research on interference effect of the canard tip vortex is needed to fully understand its impact on the dynamic characteristics of the aircraft.

Effect of Landing Gear.- Incremental values of drag are presented in figure 23 for the nose landing gear, main landing gear, and wheel fairings. These incremental values may be added or subtracted from the basic configuration drag values to obtain the appropriate drag curve for that particular configuration. Values of trimmed lift-to-drag ratios are plotted in figure 24 for various configurational changes. Starting with a baseline configuration that has leading-edge droop, nose gear retracted, wheel fairings off, and a mid c.g. location, a maximum L/D value of 12.6 was obtained. Increases in L/D_{max} were obtained by moving c.g. aft by 10-percent c ($L/D_{max} = 13.1$), adding wheel fairings ($L/D_{max} = 14.1$), and removing the main landing gear ($L/D_{max} = 15.8$).

Effect of Winglets.- Results of tests conducted with the lower and upper winglets removed are shown in figure 25. The data of figure 25 indicate that the lower winglet contributed to pitch stability in the angle-of-attack range from 6° to 14°. Incremental drag characteristics are shown in figure 26 using the winglets-off configuration as a baseline. The data of figure 26 indicate that the winglets provided drag reduction for lift coefficients above $C_L = 1.0$, which corresponds to climb. At cruise-lift coefficients, the winglets produced a drag penalty. Effect of winglets on lateral-directional characteristics will be discussed in a later section.

Lateral-Directional Characteristics

Historically, canard configurations are inherently weak in directional stability and control due to the short moment arm to the vertical tail. Lateral-directional stability derivatives, calculated from tests at $\beta = -5°$ and +5°, are presented in figure 27 for the basic configuration. The data of figure 27 indicate that the basic configuration was directionally stable at low angles of attack. Starting at about $\alpha = 12°$, directional stability of the configuration decreased with increasing angle of attack and reached unstable values at about $\alpha = 19°$. In an effort to improve the directional stability, larger winglets which were 50-percent larger in area were tested. The effect of the winglets are shown in figure 28 which presents data of the basic winglet configuration, the winglets removed configuration, and also the larger-sized winglet configuration. The data of figure 28 indicates that the configuration without winglets was directionally unstable throughout the angle-of-attack range tested. The large winglets, which were 50-percent larger than the original winglets, provided about a 50-percent increase in the contribution to directional stability and provided a positive margin of C_{n_β} throughout the angle-of-attack range tested.

As shown in figures 29 and 30, aileron- and rudder-control effectiveness of the present configuration are compared to the control effectiveness of a representative conventional configuration (reference 4). The data of figures 29 and 30 indicate that the present configuration exhibited significantly less rudder effectiveness than the conventional configuration. As would be expected for the canard arrangement the present configuration, which has ailerons located on the inboard part of the wing, exhibited favorable yaw effects with aileron deflection. Both aileron and rudder effectiveness of the present configuration decreased significantly above $\alpha = 15°$.

Boundary-Layer Transition Study

Boundary-Layer Transition.- During flight conditions in rain, pilot reports of this configuration have indicated a nose-down pitch-trim characteristic. To determine whether this characteristic was related to early transition of the boundary layer, the extent of natural laminar flow on the aircraft and the effect of loss in laminar flow were investigated. A chemical sublimation technique (reference 7) was used to determine the boundary-layer transition on the canard, wing, and winglets. The technique involved preparing the model by spraying a coat of chemical film on the model surface, starting the wind-tunnel airflow, and observing the line of demarcation which denoted transition. This line of demarcation forms a transition line because the surface chemicals sublimate at a higher rate in the turbulent boundary-layer.

The results of this transition study were obtained at a model angle of attack of 1.5° and at a Reynolds number of 1.60 million based on c. As indicated by the photographs of figure 31, transition was located at 55-percent chord of the canard, 65-percent chord of the wing, and 60-percent chord of the winget. Although the tests were conducted in a wind tunnel which has a turbulent factor of 1.1, and at a test Reynolds number which was less than cruise flight Reynolds number, these transition results were confirmed by flight tests as reported in reference 10. The large extent of laminar flow can be attributed to the aircraft's composite construction which allowed for smooth airfoil contours so that full theoretical values of laminar flow can be achieved.

Effect of Transition on Canard. As indicated by the flow visualization using sublimating chemicals, the boundary-layer transition was found to be at 55-percent chord on the canard. Tests were conducted to determine the effects of early transition on the canard as would happen, for example, when insects accumulate along the leading-edge or when flying in rain. In order to artificially induce early transition, carborundum grit was applied to the canard at 5-percent chord in accordance with reference 11. In addition, rain effects were

simulated using water spray from a horizontal boom mounted in the wind tunnel about 4 chord lengths ahead of the canard (see figure 32). The water spray boom covered only one side of aircraft and ejected water spray at a rate of 1 gallon per minute. This water flow rate would correspond to very heavy rain conditions.

Results of tests with transition grit on the canard, shown in figure 33(a), indicate that fixed transition at 5-percent chord decreased the lift-curve slope of the canard by about 30-percent. This reduction in canard lift resulted in nose-down pitching-moment increments. In addition, the canard-balance data shown in figure 33(b) indicate significant drag increments. An examination of the chordwise pressure distribution on the canard, shown in figure 34, indicates that the loss in lift due to fixed transition resulted from premature trailing-edge separation which was probably due to thickening of the boundary layer and the sharp pressure recovery to the trailing edge. This premature separation near the trailing-edge results in decreased elevator effectiveness as shown in figure 35. This decreased elevator effectiveness can become significant in flight conditions with rain where loss of laminar flow would occur and significant changes in elevator trim would be required.

Results from water spray tests on the canard, shown in figure 36, indicate that rain effects were similar to results of early transition on the canard; that is, the lift-curve slope was reduced and drag increased. Note that only half of the canard was immersed in water spray; therefore, if the canard was fully immersed, the results would be in closer agreement with the results of the transition-fixed canard. Thus, the water spray tests confirm the analogy of the effects of rain and loss of laminar flow on the canard aerodynamic performance.

Concluding Remarks

A full-scale wind-tunnel investigation has been conducted to determine the longitudinal and lateral-directional aerodynamic characteristics of an advanced canard-configured general-aviation airplane. A summary of the significant results of this investigation is listed as follows:

1. The canard on this configuration was effective in providing increased stall departure resistance due to the limiting effect of angle of attack on the canard contribution to pitching moments.

2. The canard airfoil section characteristics can strongly affect the configuration's stall and post-stall characteristics.

3. Results from testing the canard in a lower position indicated that although the configuration exhibited slightly less pitch stability, the low canard on this configuration appears feasible in terms of stability, control, and performance.

4. The outboard wing leading-edge droop provided attached flow at the wingtip to a higher angle of attack and increased pitch stability at low to moderate angles of attack.

5. From tests using a chemical sublimation technique, the boundary-layer transition was found to be at 55-percent chord of the canard. Fixing transition near the leading-edge resulted in a significant reduction of lift due to flow separation near the trailing edge of the canard, and subsequently a nose-down trim change and loss of elevator effectiveness.

References

1. Rutan, Burt: Development of a Small, High Aspect-Ratio Canard Aircraft. Society of Experimental Test Pilots Symposium, September 22-25, 1976.

2. Foa, Joseph V.: Proportioning a Canard Airplane for Longitudinal Stability and Safety Against Stall. Journal of the Aeronautical Sciences, pp. 523-528 December, 1942.

3. Kelling, F. H.: Experimental Investigation of a High-Lift Low-Drag Aerofoil. ARC CP1187, 1971.

4. Staff of the Langley Research Center: Exploratory Study of the Effects of Wing Leading-Edge Modifications on the Stall/Spin Behavior of a Light General Aviation Airplane. NASA TP 1589, 1979.

5. Newsom, William A., Jr.; Satran, Dale R.; and Johnson, Joseph L.: Effects of Wing Leading-Edge Modifications on a Full-Scale Low-Wing General Aviation Airplane. NASA TP 2011, June 1982.

6. DeFrance, Smith J.: The NASA Full-Scale Tunnel. NACA TR 459, 1933.

7. Main-Smith, J. D.: Chemical Solid as Diffusable Coating Film for Visual Indication of Boundary-Layer Transition in Air and Water. ARC R and M 2755, 1950.

8. Theodorsen, Theodore; and Silverstein, Abe: Experimental Verification of the Theory of Wind-Tunnel Boundary Interference. NACA TR-478, 1934.

9. Heyson, Harry H.: Use of Superposition in Digital Computers to Obtain Wind-Tunnel Interference Factors for Arbitrary Configurations, with Particular Reference to V/STOL Models. NASA TR 302, 1969.

10. Holmes, B. J.: Natural Laminar Flow Research for General Aviation Application. ICAS paper no. 82-5.1.1, August 1982.

11. Braslow, Albert L.; and Knox, Eugene C.: Simplified Method for Determination of Critical Height of Distributed Roughness Particles for Boundary-Layer Transition at Mach Numbers from 0 to 5. NACA TN 4363, 1958.

TABLE I.- GEOMETRIC CHARACTERISTICS OF THE MODEL

Reference Dimensions:

S, ft^2	53.60
b, ft	22.17
c, ft	2.58

Wing:

Area, ft^2	53.60
Span, ft	22.17
Aspect Ratio	9.17
Root chord, centerline, ft	3.47
Tip chord, ft	1.33
Taper ratio	0.38
Sweep, c/4, deg	25.7
Dihedral, deg	-4
Root incidence, BL32, deg	1.2
Tip incidence, deg	-1.8
Airfoil section	GA(W)-1 (modified)
Aileron - area, total, ft^2	4.0
span, per side, ft	3.33
chord, percent wing chord	20

Canard:

Area, ft^2	12.82
Span, ft	11.83
Aspect Ratio	10.92
Chord, ft	1.08
Taper ratio	1.00
Sweep, deg	0
Airfoil	GU 25-5 (11) 8
Elevator hinge-line location, percent chord	70

Winglet:

Area, total, ft^2	6.96
Span, per side, ft	3.09
Root chord, ft	1.67
Tip chord, ft	0.58
Sweep, c/4, deg	26.3

WING		CANARD		WINGLET		L.E. DROOP	
$(x/c)_u$	$(x/c)_l$	$(x/c)_u$	$(x/c)_l$	$(x/c)_u$	$(x/c)_l$	$(x/c)_u$	$(x/c)_l$
0	.02	0	.01	0	.02	-.065	.050
.005	.05	.005	.05	.02	.10	-.060	.020
.02	.10	.02	.15	.05	.30	-.045	.030
.05	.25	.05	.35	.10	.50	-.015	
.10	.40	.10	.50	.30	.70	.030	
.175	.55	.175	.625	.50	.90		
.25	.65	.25	.65	.75			
.40	.75	.40	.75	.90			
.55	.85	.50	.85	.95			
.65	.95	.65	.95				
.75		.75					
.85		.85					
.95		.95					

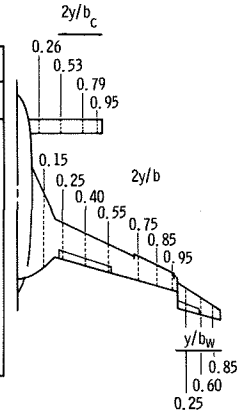

TABLE II.- PRESSURE ORIFICE LOCATIONS

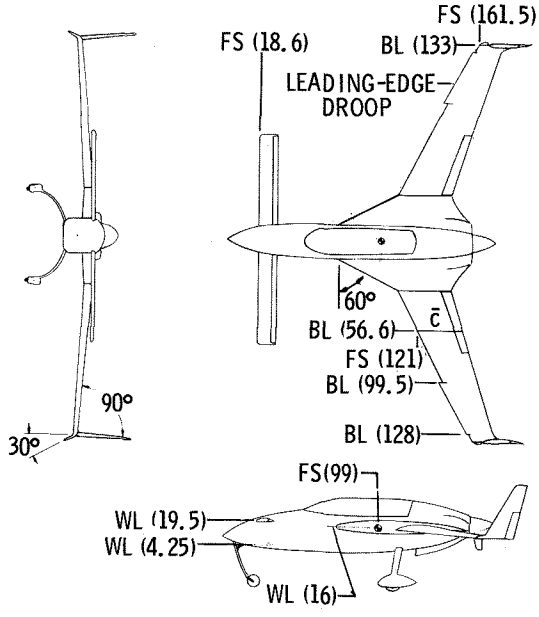

(a) Three-view drawing

Figure 1.- Geometric characteristics of model. Dimensions in inches.

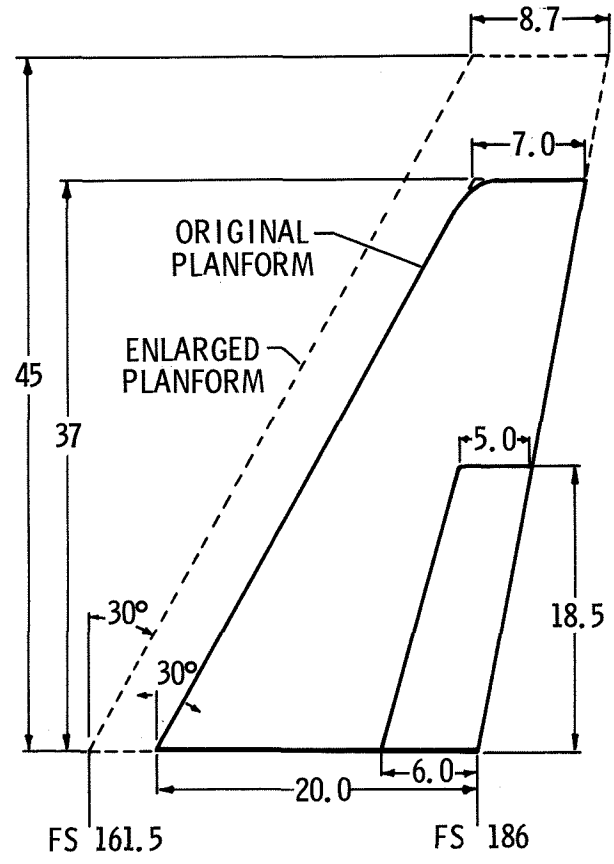

(b) Winglet

Figure 1.- Continued

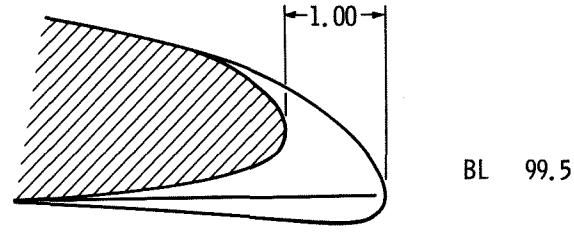

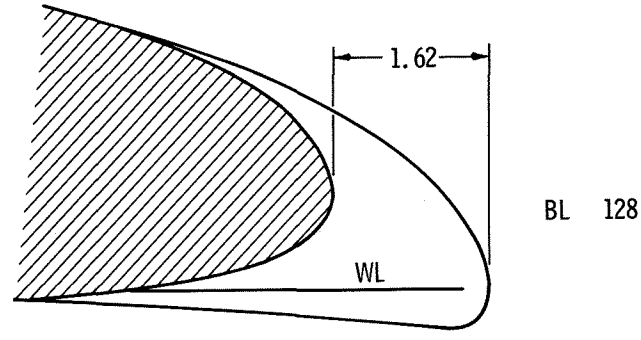

(c) Leading-edge droop

Figure 1.- Concluded

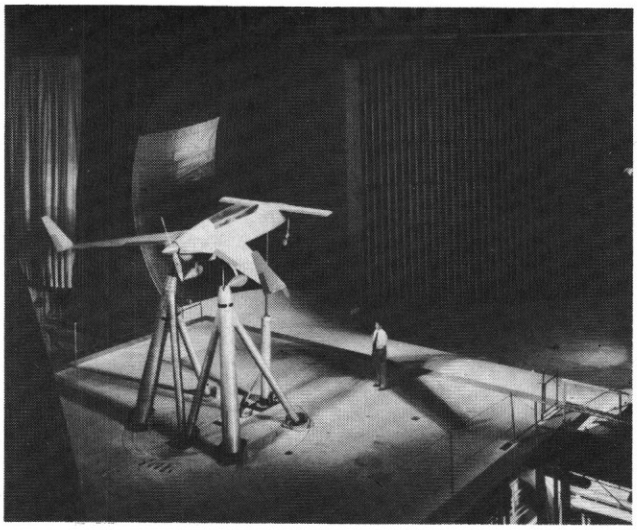

Figure 2.- Model installed in the Langley 30-by 60-Foot Wind Tunnel.

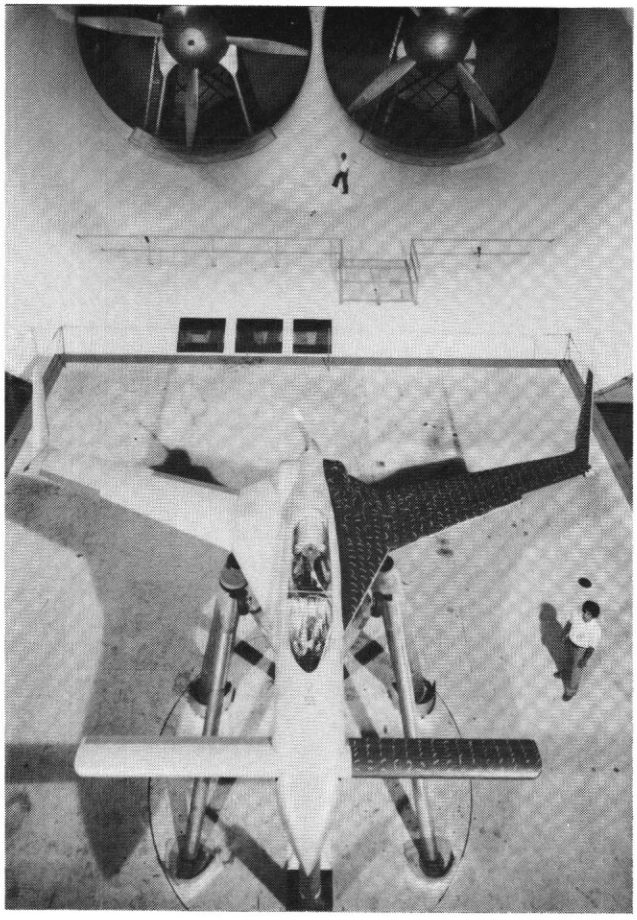

Figure 3.- Top view of model.

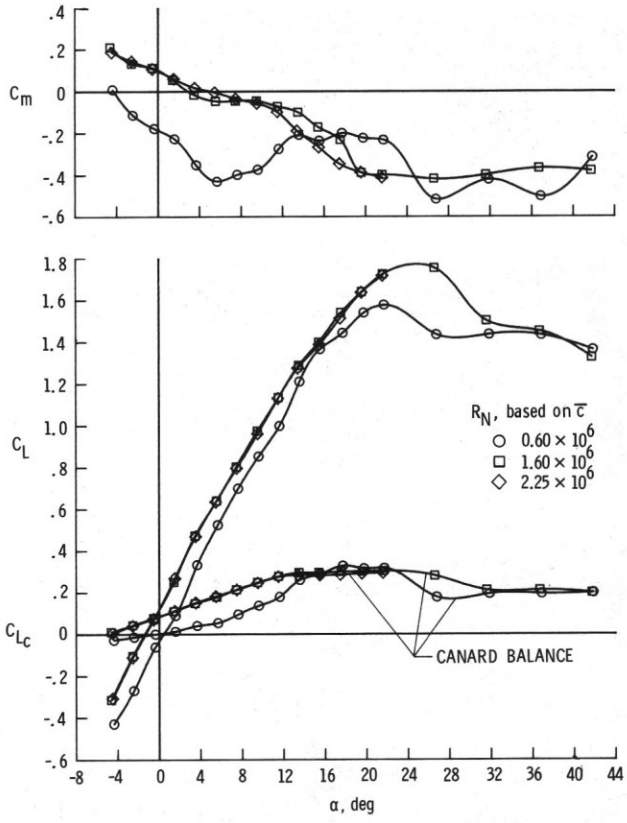

Figure 4.- Effect of Reynolds number. Leading-edge droop off.

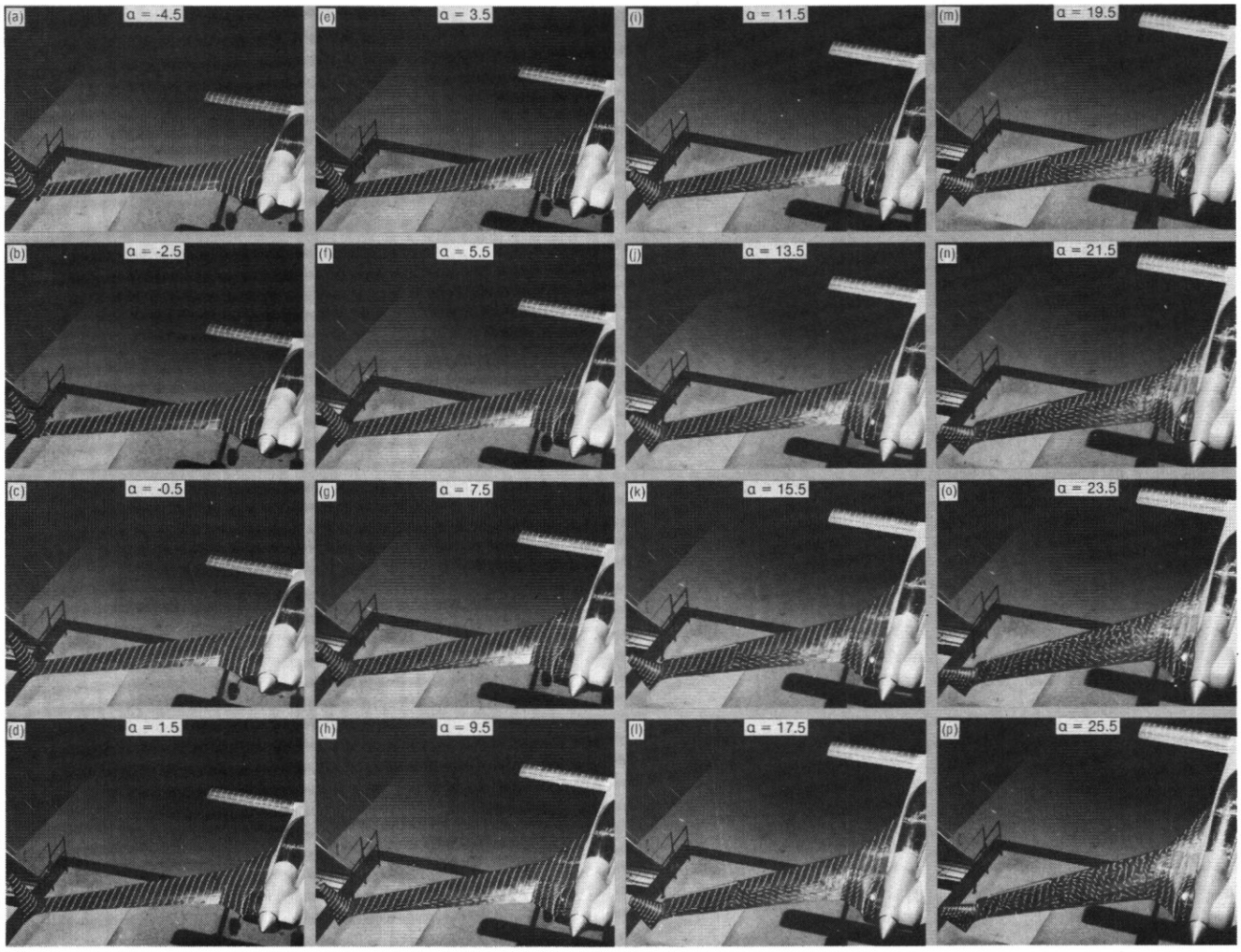

Figure 5.- Effect of angle of attack on the surface flow patterns of the basic configuration.

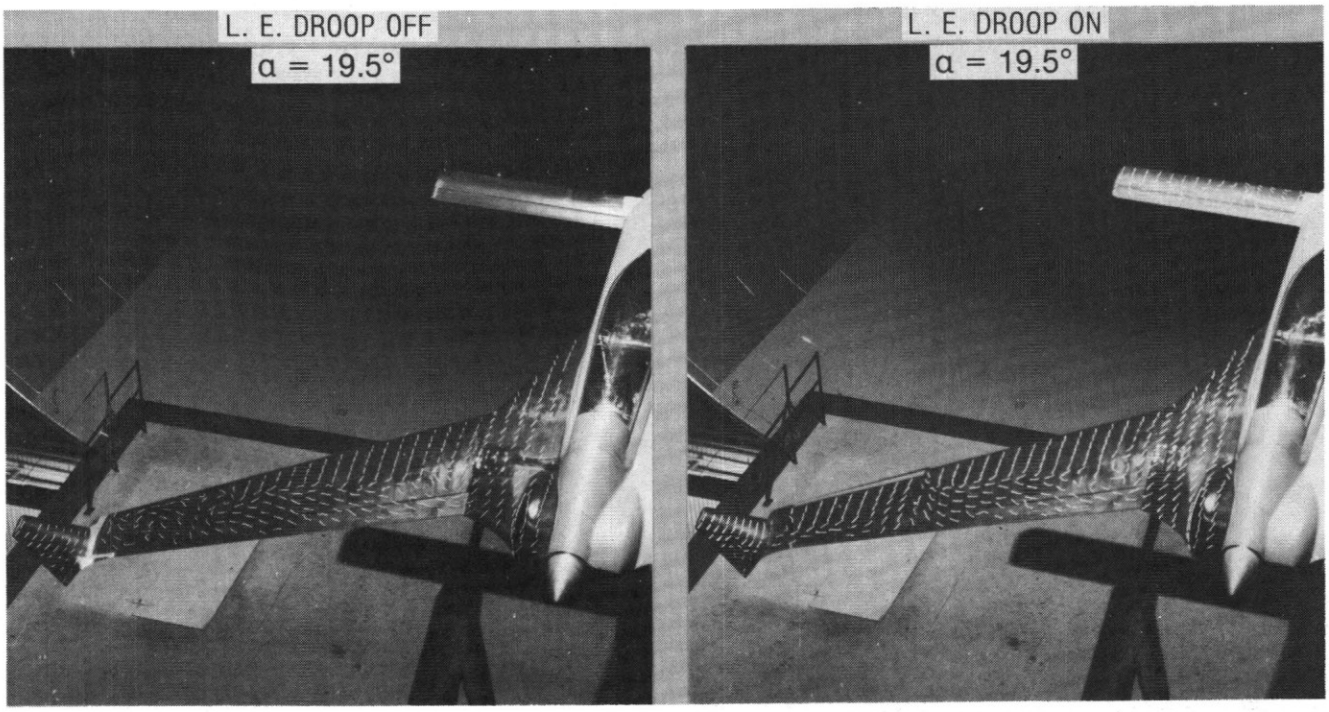

Figure 6.- Effect of leading-edge droop. α = 19.5°.

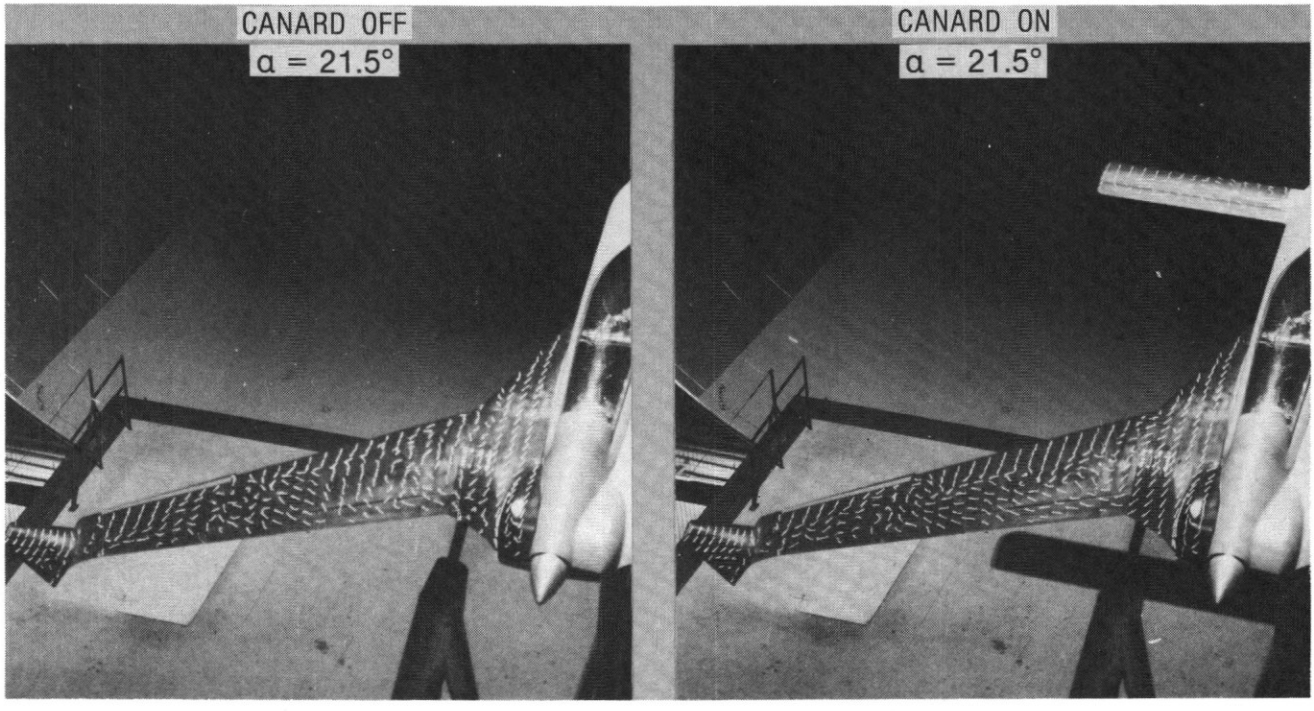

Figure 7.- Effect of canard downwash on main wing. α = 21.5°.

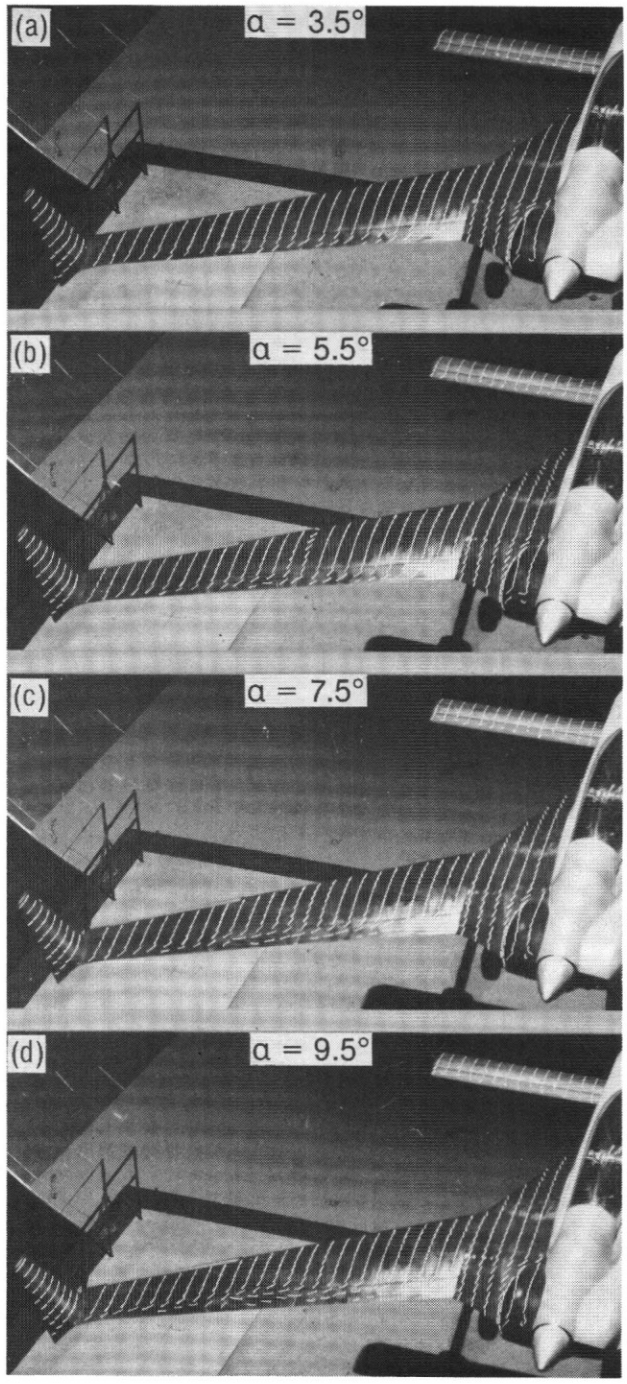

Figure 8.- Effect of canard tip vortex interference on main wing. Canard in low position.

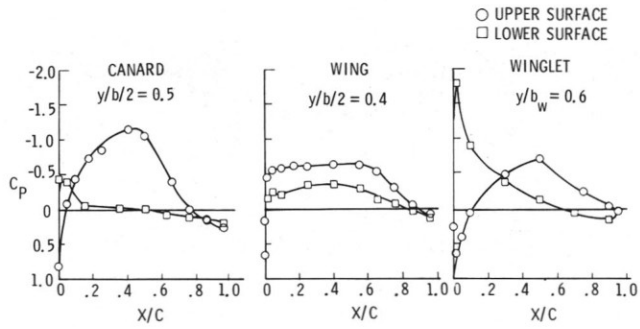

Figure 9.- Chordwise pressure distributions. α = 1.5°.

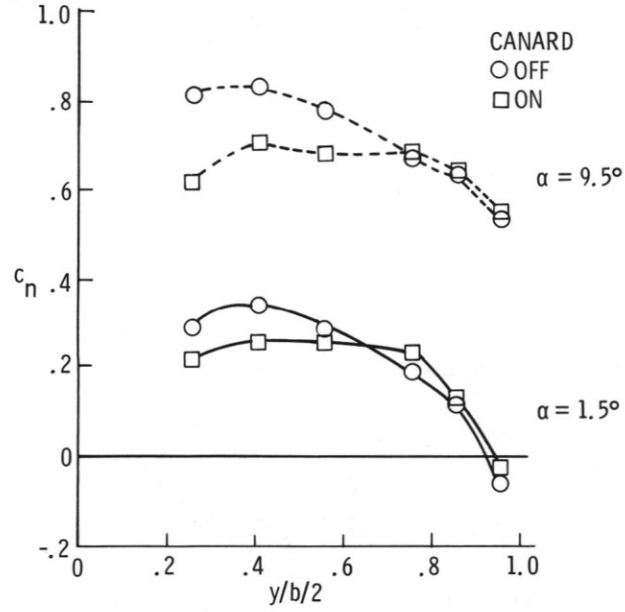

Figure 10.- Effect of canard on spanload distribution of wing.

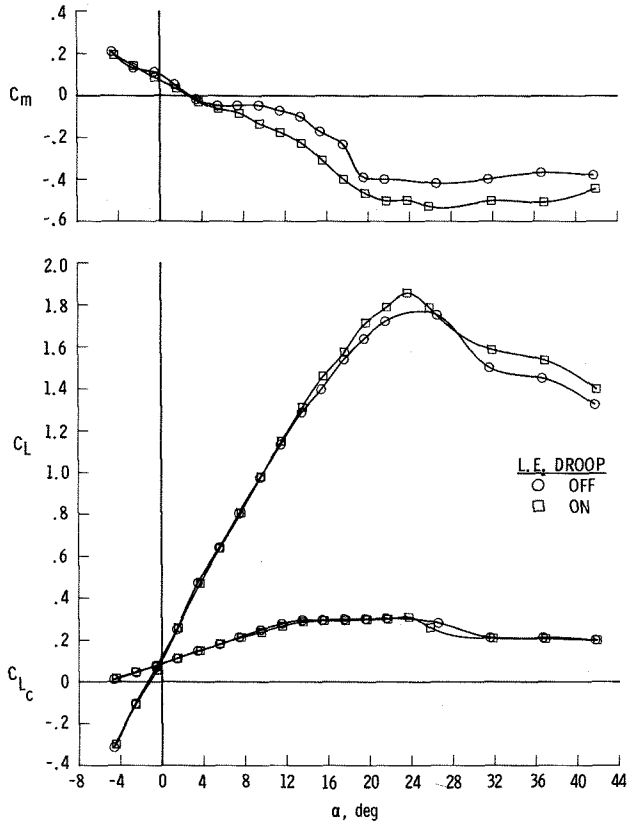

Figure 11.- Effect of leading-edge droop on longitudinal characteristics.

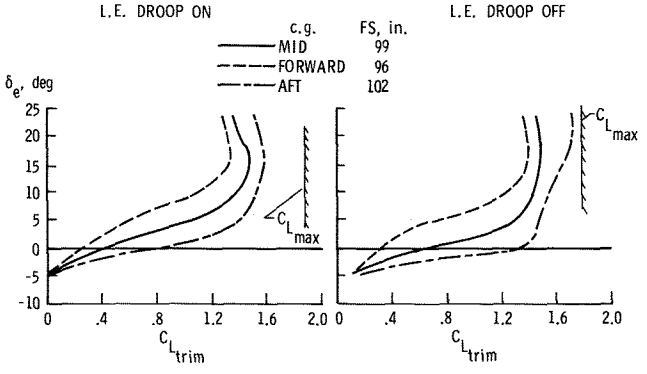

Figure 12.- Effect of leading-edge droop on elevator deflection required for trim.

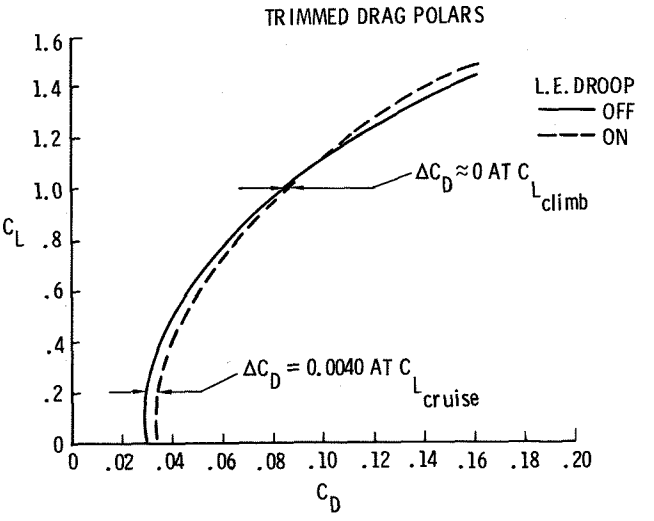

Figure 13.- Effect of leading-edge droop on drag characteristics.

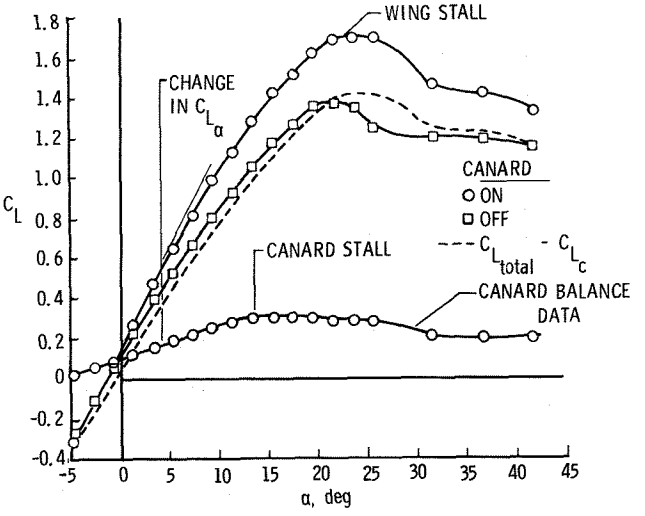

(a) Lift characteristics

Figure 14.- Effect of canard on basic configuration.

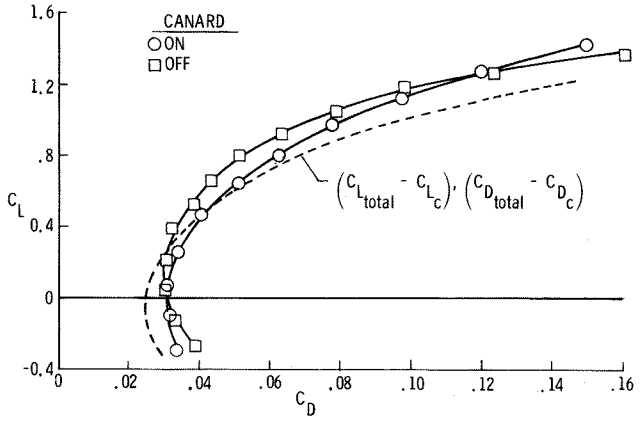

(b) Drag characteristics

Figure 14.- Continued

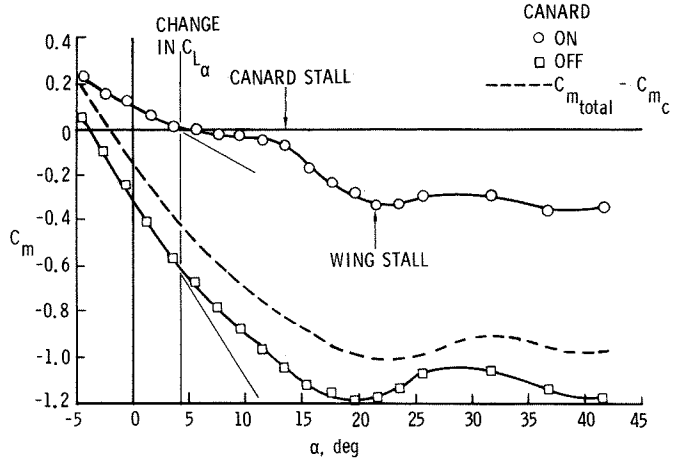

(c) Pitching-moment characteristics

Figure 14.- Concluded

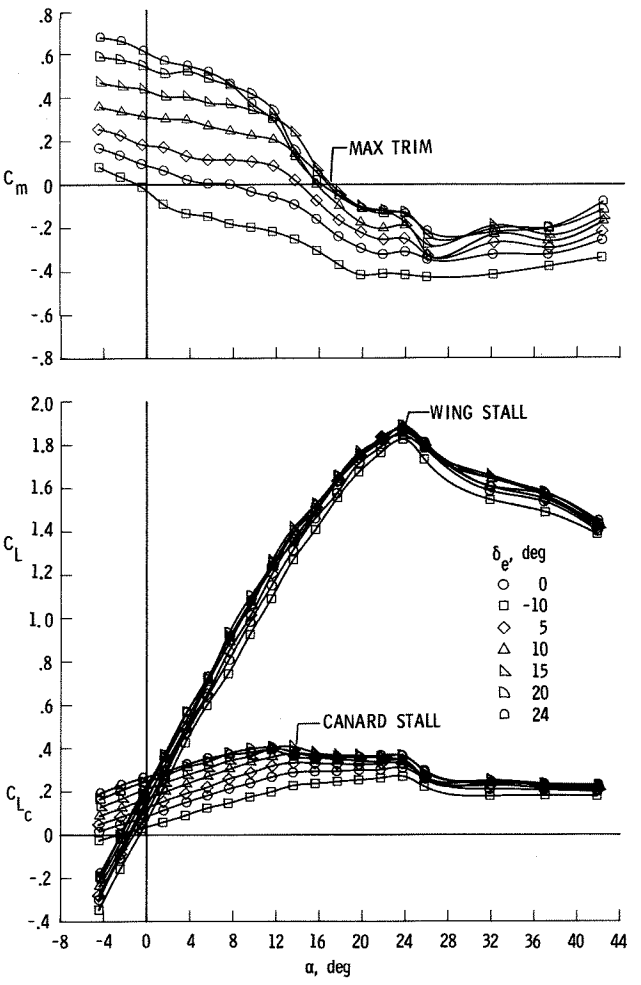

Figure 15.- Effect of elevator deflection on basic configuration. Aft-c.g., FS102.

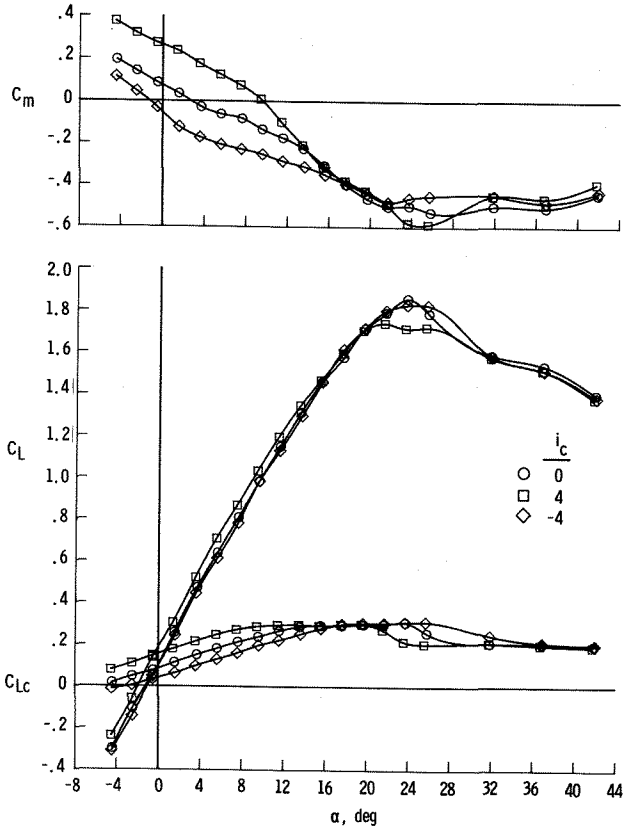

Figure 16.- Effect of canard incidence. Basic configuration.

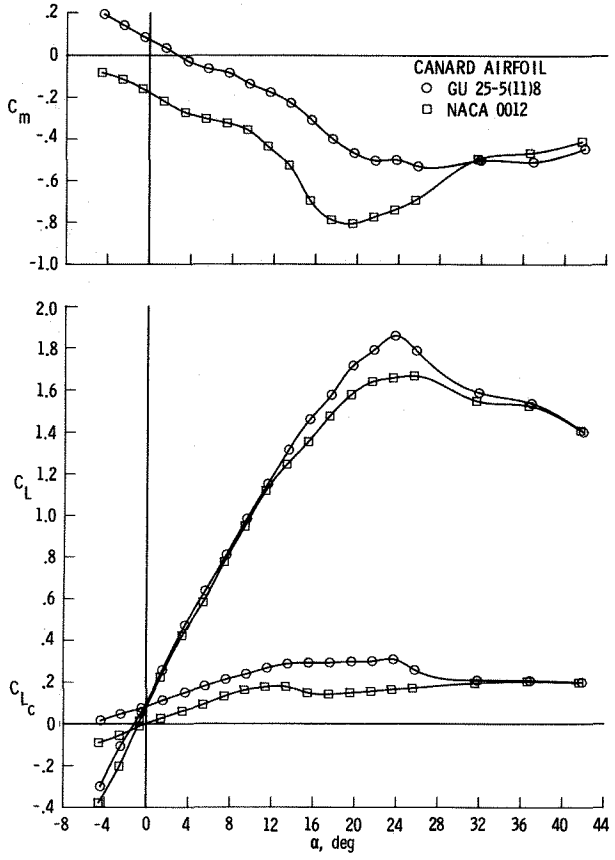

Figure 18.- Effect of canard airfoil on longitudinal characteristics.

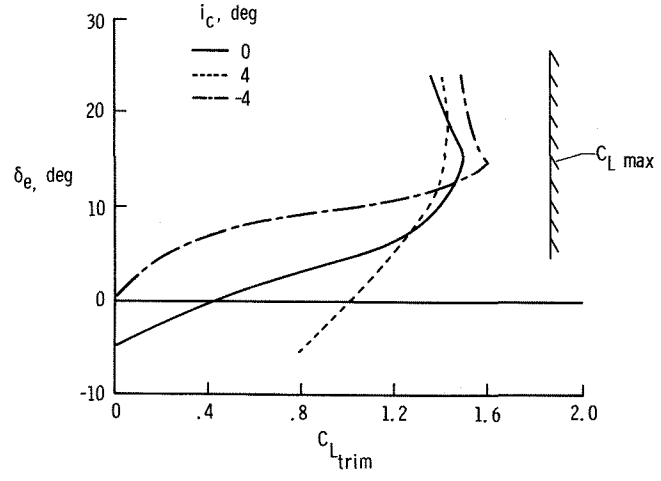

Figure 17.- Effect of canard incidence on elevator deflection required to trim.

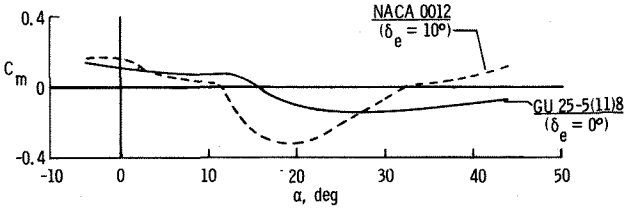

Figure 19.- Effect of canard airfoil on longitudinal stability of configuration with aft-c.g.

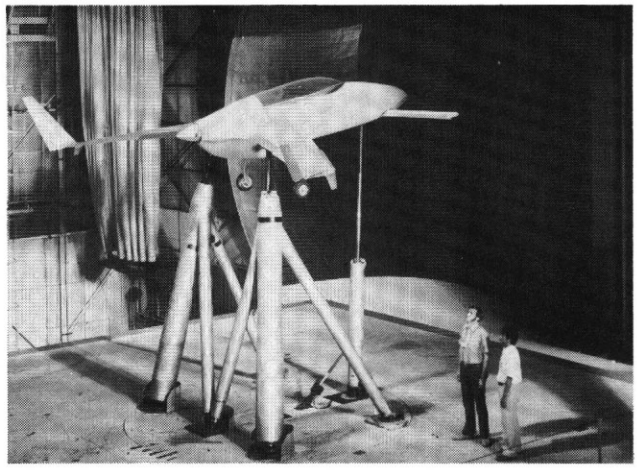

Figure 20.- View of canard in low position.

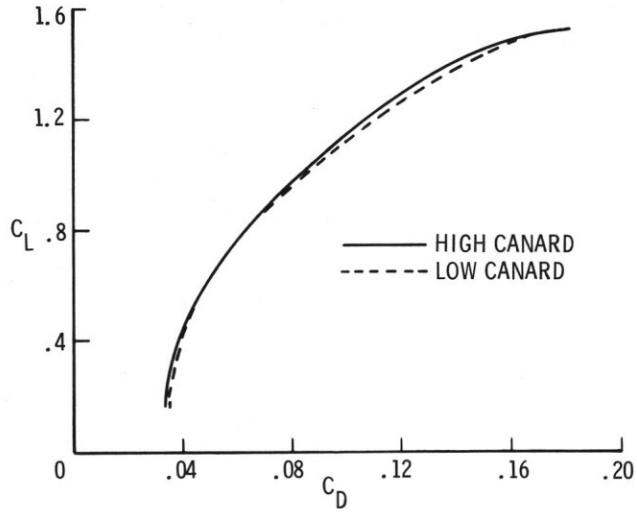

Figure 22.- Effect of canard height on trimmed drag.

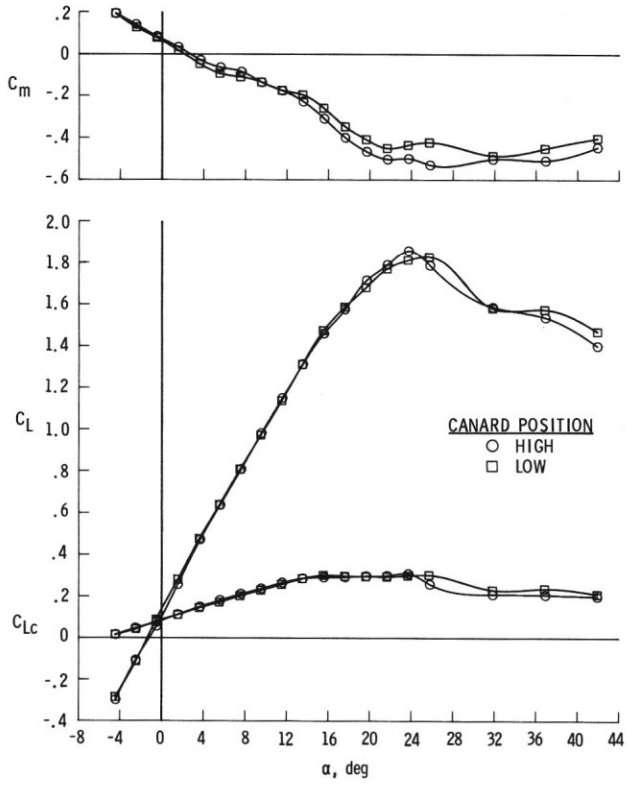

Figure 21.- Effect of canard height on the longitudinal aerodynamic characteristics.

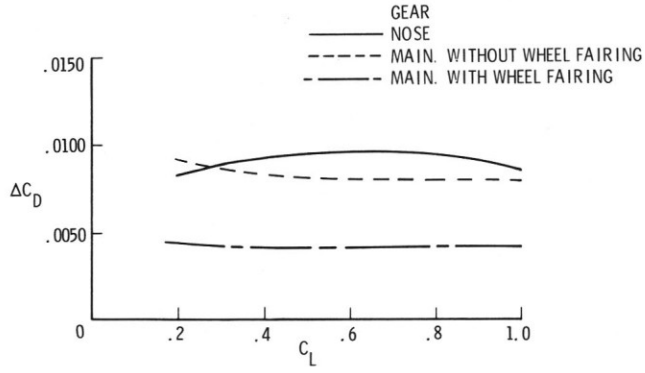

Figure 23.- Incremental drag characteristics of various landing gear arrangements.

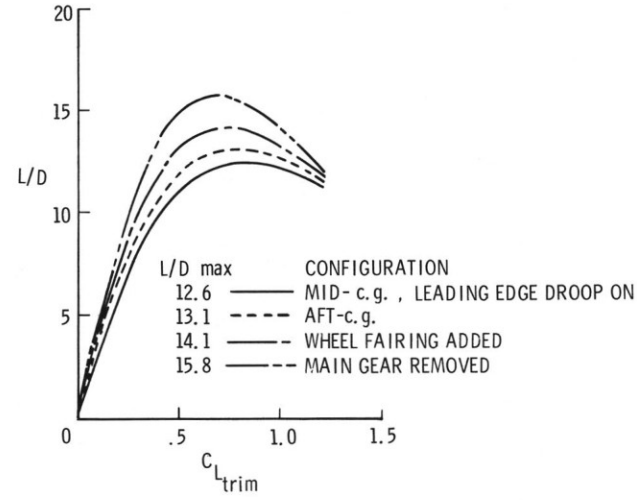

Figure 24.- Trimmed lift-to-drag characteristics for various configuration changes.

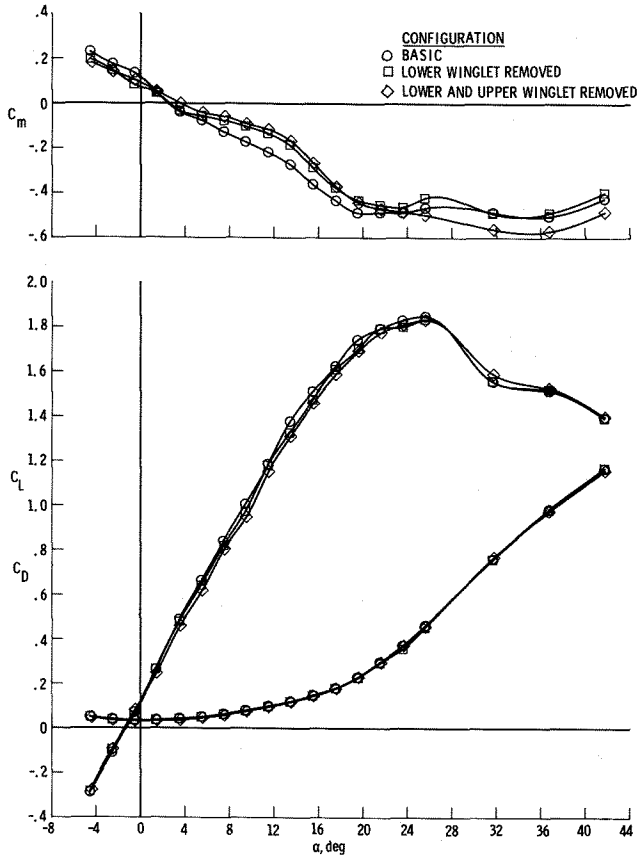

Figure 25.- Effect of winglets on longitudinal characteristics of basic configuration.

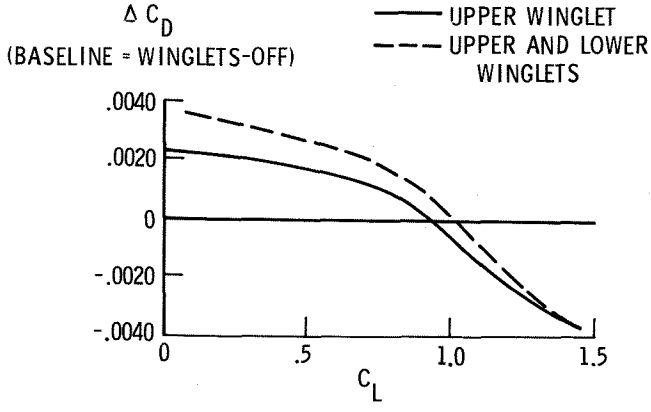

Figure 26.- Effect of winglets on drag.

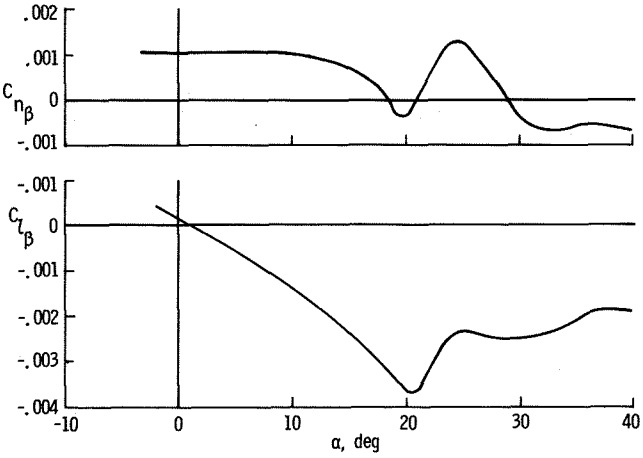

Figure 27.- Lateral-directional characteristics of the basic configuration.

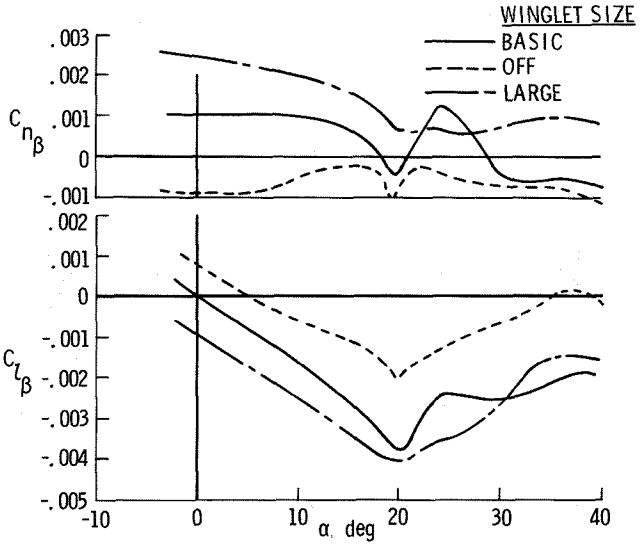

Figure 28.- Effect of winglets on lateral-directional characteristics.

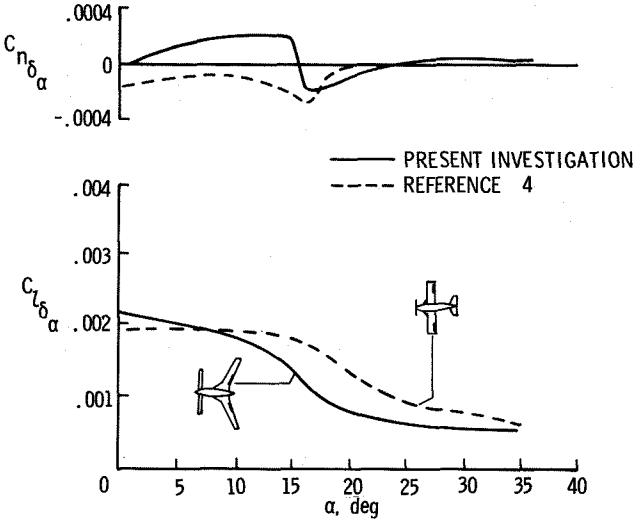

Figure 29.- Aileron effectiveness.

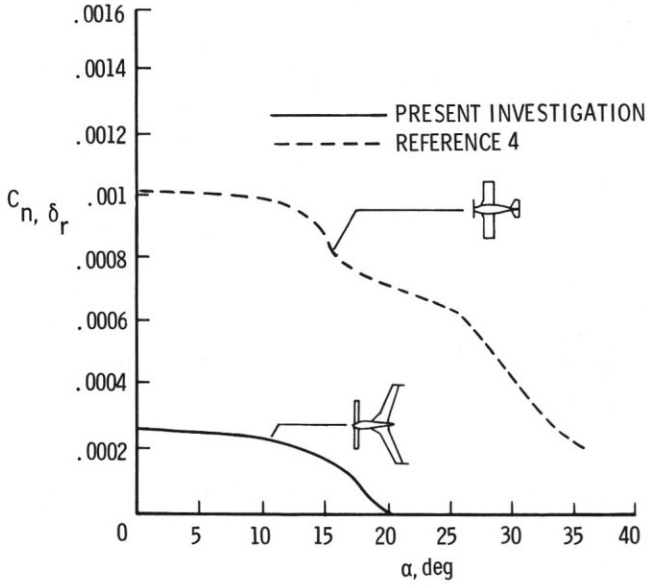

Figure 30.- Rudder effectiveness.

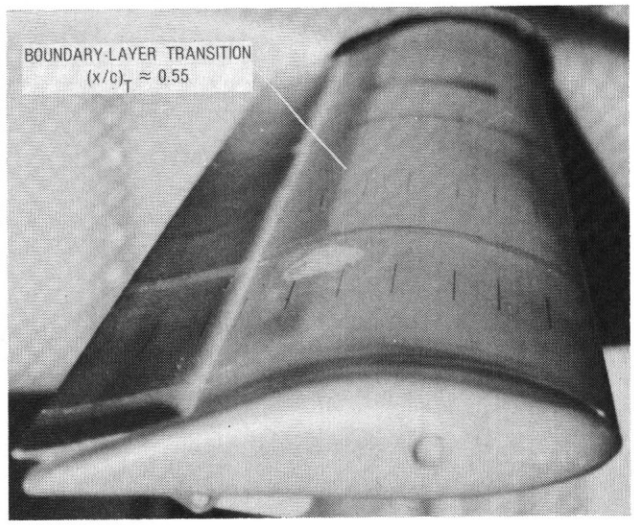

(b) Canard

Figure 31.- Continued.

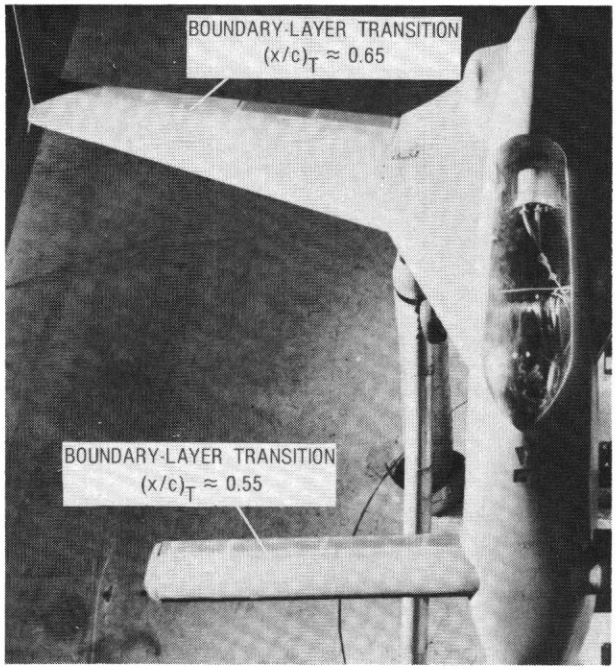

(a) Top view of wing and canard

Figure 31.- Flow visualization using sublimating chemicals to show boundary-layer transition. $\alpha = 1.5°$.

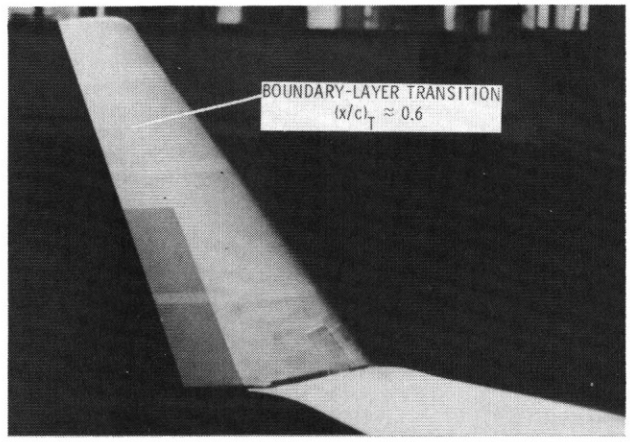

(c) Winglet

Figure 31.- Concluded.

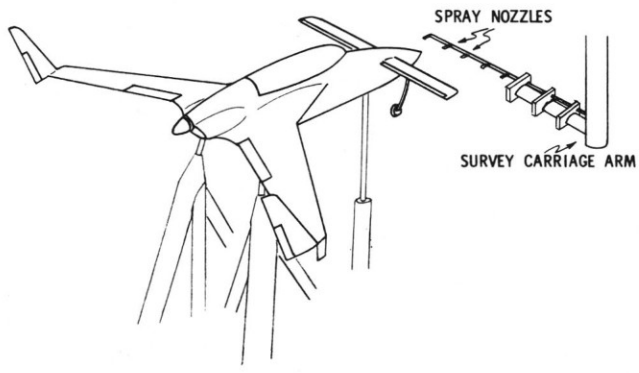

Figure 32.- Sketch of water-spray apparatus.

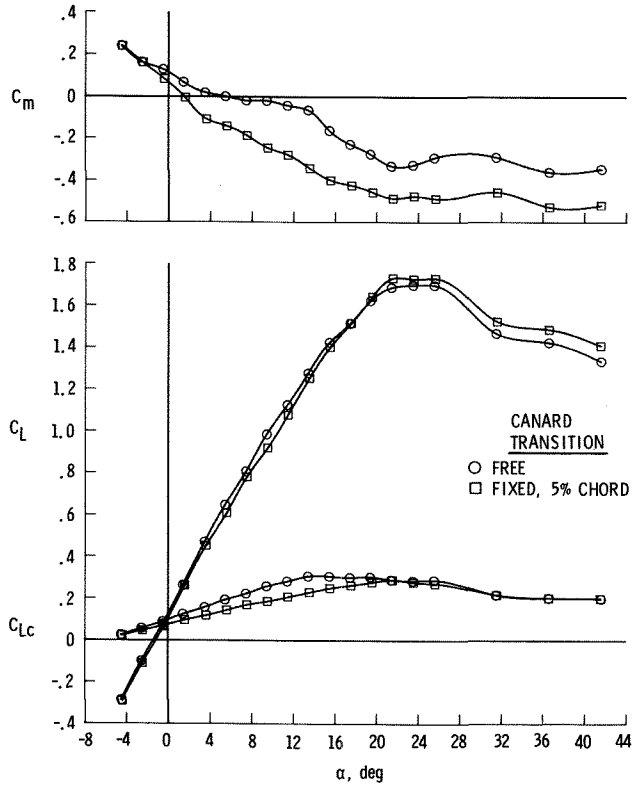

(a) Total airplane characteristics

Figure 33.- Effect of fixing transition on canard.

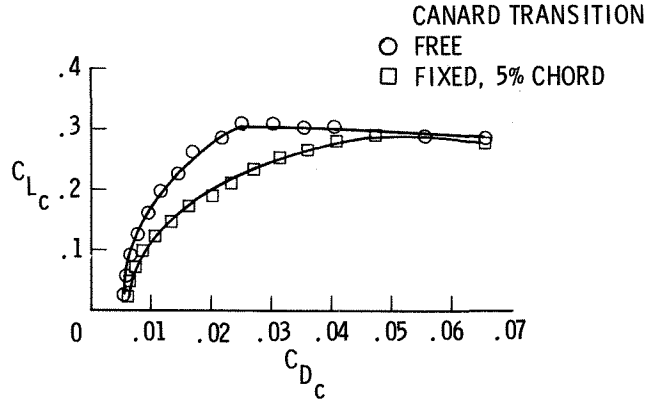

(b) Canard balance data

Figure 33.- Concluded.

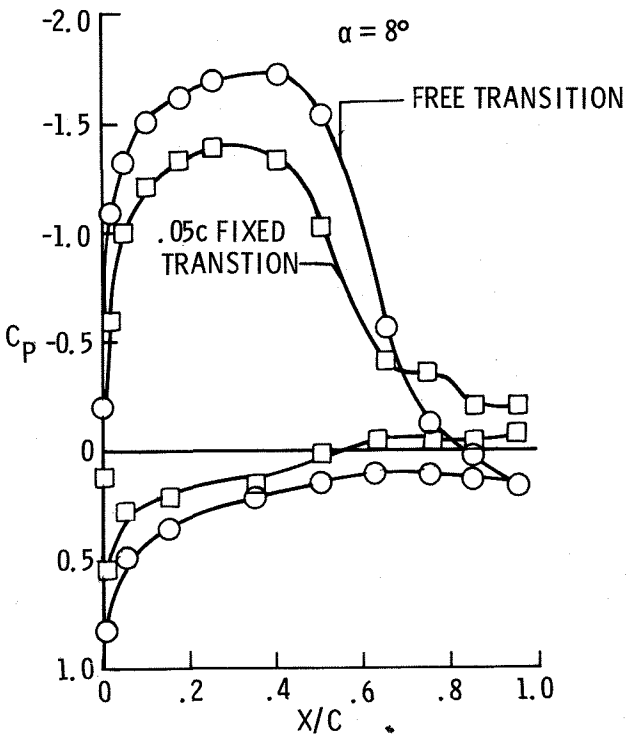

Figure 34.- Effect of fixed transition on the chordwise pressure distribution of the canard. α = 8°.

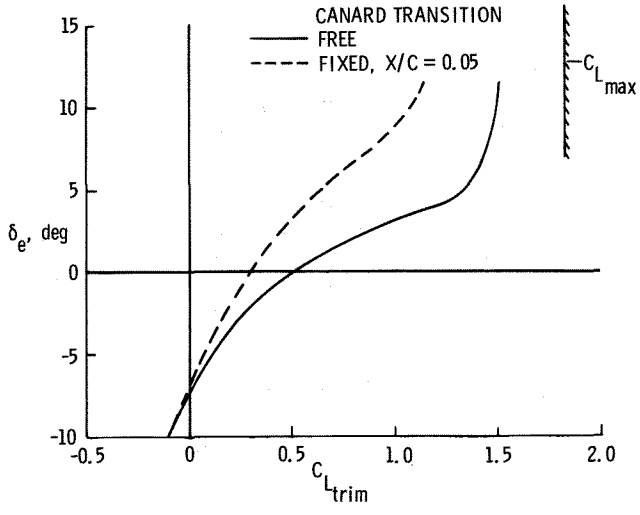

Figure 35.- Effect of canard transition on elevator effectiveness.

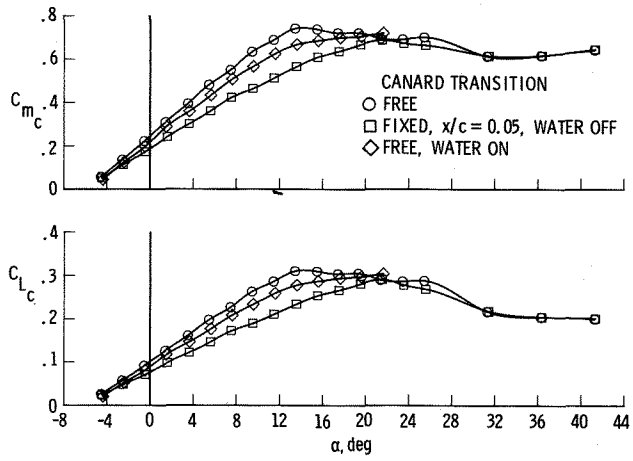

(a) Lift and pitching moments

Figure 36.- Effect of water spray on canard aerodynamics.

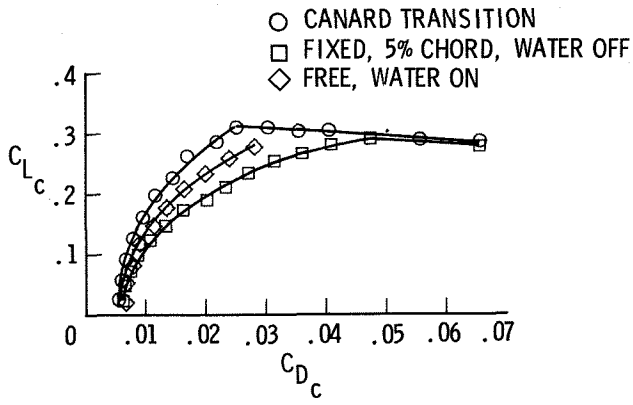

(b) Drag characteristics

Figure 36.- Concluded.